



Paper

Cite this article: Kassab CM, Licht KJ, Petersson R, Lindbäck K, Graly JA, Kaplan MR (2020). Formation and evolution of an extensive blue ice moraine in central Transantarctic Mountains, Antarctica. *Journal of Glaciology* 66(255), 49–60. <https://doi.org/10.1017/jog.2019.83>

Received: 22 April 2019

Revised: 14 October 2019

Accepted: 15 October 2019

First published online: 11 November 2019

Key words:

Blue ice; ground-penetrating radar; moraine formation

Author for correspondence:

Christine M. Kassab,

E-mail: ckassab@iupui.edu

Formation and evolution of an extensive blue ice moraine in central Transantarctic Mountains, Antarctica

Christine M. Kassab¹ , Kathy J. Licht¹, Rickard Petersson², Katrin Lindbäck³, Joseph A. Graly^{1,4} and Michael R. Kaplan⁵

¹Department of Earth Sciences, Indiana University-Purdue University Indianapolis, 723 W Michigan St, SL118, Indianapolis, IN 46202, USA; ²Department of Earth Sciences, Uppsala University, Geocentrum, Villav. 16, 752 36, Uppsala, Sweden; ³Norwegian Polar Institute, Fram Centre, P.O. Box 6606 Langnes, NO-9296, Tromsø, Norway; ⁴Department of Geography and Environmental Sciences, Northumbria University, Ellison Place, Newcastle upon Tyne, NE1 8ST, UK and ⁵Division of Geochemistry, Lamont-Doherty Earth Observatory, Palisades, New York 10964, USA

Abstract

Mount Achernar moraine is a terrestrial sediment archive that preserves a record of ice-sheet dynamics and climate over multiple glacial cycles. Similar records exist in other blue ice moraines elsewhere on the continent, but an understanding of how these moraines form is limited. We propose a model to explain the formation of extensive, coherent blue ice moraine sequences based on the integration of ground-penetrating radar (GPR) data with ice velocity and surface exposure ages. GPR transects (100 and 25 MHz) both perpendicular and parallel to moraine ridges at Mount Achernar reveal an internal structure defined by alternating relatively clean ice and steeply dipping debris bands extending to depth, and where visible, to the underlying bedrock surface. Sediment is carried to the surface from depth along these debris bands, and sublimates out of the ice, accumulating over time (>300 ka). The internal pattern of dipping reflectors, combined with increasing surface exposure ages, suggest sequential exposure of the sediment where ice and debris accretes laterally to form the moraine. Subsurface structure varies across the moraine and can be linked to changes in basal entrainment conditions. We speculate that higher concentrations of debris may have been entrained in the ice during colder glacial periods or entrained more proximal to the moraine sequence.

Introduction

With the increasing focus on how Earth's ice sheets will respond to future changes in our climate, we must gain a more thorough understanding of how they have responded during previous climate fluctuations. Terrestrial geologic records of ice-sheet history are typically discontinuous (i.e. Denton and others, 1989; Staiger and others, 2006; Bromley and others, 2010; Todd and others, 2010; Ackert and others, 2011, 2013; Joy and others, 2014) and so we often turn to distal glacial deposits in offshore sediment cores to make inferences about past ice-sheet characteristics prior to the Last Glacial Maximum (i.e. Krissek and others, 2007; McKay and others, 2009). For instance, distinct lithofacies in a sediment core collected in the Ross Sea record successive glacial advances and retreats on the continental shelf (Krissek and others, 2007). This provides important information about what happens near the ice-sheet margin, but it cannot provide information about the interior of the ice sheet.

One requirement to preserve a continuous terrestrial record of ice-sheet history is a site with relatively little change in ice-sheet thickness (Bader and others, 2017; Kaplan and others, 2017). Sites that fulfill this requirement can potentially provide information on ice dynamics over multiple glacial-interglacial cycles and better constrain conditions in the interior of the ice sheet that are critical in evaluating numerical model predictions of ice-sheet stability (i.e. Jamieson and others, 2010; Pattyn, 2010; Whitehouse and others, 2012; Golledge and others, 2013).

Blue ice areas and associated deposits, located mostly in mountainous regions of Antarctica, are sites that have the potential to preserve long term records of ice-sheet changes. They are characterized by exposed glacier ice at the surface and a negative surface mass balance as a result of high sublimation (Bintanja, 1999). Mapping via satellite imagery shows that blue ice areas cover ~1–2% of Antarctica (Winther and others, 2001; Hui and others, 2014). These areas have been noted for the abundance of meteorites (e.g. Whillans and Cassidy, 1983; Cassidy and others, 1992; Harvey, 2003; Zekollari and others, 2019) and for the potential paleoclimate record contained within the ice (e.g. Moore and others, 2006; Sinisalo and others, 2007; Korotikikh and others, 2011; Spaulding and others, 2013; Higgins and others, 2015). Researchers have used ground-penetrating radar (GPR) in some blue ice areas to link the internal stratigraphy to a known isotopic paleoclimate record (i.e. Winter and others, 2016) or ice flow history (i.e. Campbell and others, 2013). Other researchers have also used GPR in other ice marginal regions in Antarctica to investigate the internal stratigraphy of debris

© The Author(s) 2019. This is an Open Access article, distributed under the terms of the Creative Commons Attribution licence (<http://creativecommons.org/licenses/by/4.0/>), which permits unrestricted re-use, distribution, and reproduction in any medium, provided the original work is properly cited.

cambridge.org/jog

covered glaciers (i.e. Shean and Marchant, 2010; Mackay and others, 2014) and rock glaciers (i.e. Fukui and others, 2008).

In places where sediment accumulates on the surface of blue ice areas either as a result of rockfall or emerging from the ice through sublimation, blue ice moraines can develop. Although extensive blue ice moraines have the potential for recording long-term changes in ice dynamics and basal conditions of entrainment (Graly and others, 2018b), there is a limited understanding on how these types of moraines form and evolve over time. We seek to build upon this work by studying a particularly large blue ice moraine in the central Transantarctic Mountains, where sediment is accumulating on the surface as the ice sublimates. Here we describe new findings based on GPR data from the Mount Acheron moraine along upper Law Glacier that reveals the internal stratigraphy of this blue ice moraine, and we develop a model explaining the temporal evolution of moraine formation. We use the changes in characteristics of the internal stratigraphy to hypothesize how the architecture can be linked to changes in ice flow and basal conditions through time.

Background

Blue ice areas/moraines

Blue ice areas can form in a variety of places on an ice sheet and are characterized by a negative mass balance due to high sublimation rates which expose glacier ice at the surface (Bintanja, 1999). Sinisalo and Moore (2010) classified blue ice areas into two types, open and closed, based on the absence or presence of bedrock obstacles impeding ice flow, respectively. In both systems, subsurface ice is brought to the surface as a result of sublimation, but the difference lies in whether the deepest layers reach the surface. In the absence of a barrier, the deepest/oldest layers of ice in open systems do not reach the surface. In closed systems, where ice flow encounters a bedrock obstacle and sublimation removes the ice at the surface, the deepest/oldest ice layers reach the surface, exposing the oldest ice that was previously closest to the bedrock (Sinisalo and Moore, 2010). As Corti and others (2008) show in a laboratory model, it is the combination of stresses related to ice flow around a barrier and high sublimation rates that pulls the oldest ice to the surface.

Sediment entrained subglacially or englacially in deep ice layers can be brought to the surface in blue ice areas. Moraines that form from the accumulation of sediment in blue ice areas are referred to as blue ice moraines. They range from isolated patches of debris a few m² up to 100 km². Most research on blue ice moraines has focused on the sedimentology of the moraine debris and its exposure chronology (e.g. Altmaier and others, 2010; Fogwill and others, 2011; Hein and others, 2016; Bader and others, 2017; Kaplan and others, 2017). These studies have shown that formation of blue ice moraines can occur over long time periods (>100 ka) indicating that the moraines have been stable for long periods of time (Altmaier and others, 2010; Kaplan and others, 2017). Fogwill and others (2011) noted that the stability of blue ice moraines in the Heritage Range of the Ellsworth Mountains is the result of a compressive ice flow toward the glacier margin preventing the evacuation of the sediment away from its original depositional location. They also noted a distinct dip and zigzag pattern in debris bands that form the moraine which they argued is typical of ice deformation and folding known to characterize compressive marginal zones. Other studies in the Heritage Range (Hein and others, 2016), in Queen Maud Land (Altmaier and others, 2010) and in the Transantarctic Mountains (Palmer and others, 2012; Bader and others, 2017) have noted that the sediment forming blue ice moraines is being derived subglacially and subsequently brought to the

surface. While these studies have focused mostly on the sediments exposed at the surface and chronologic history of the moraine, more research is needed to develop a better understanding of processes by which these moraines form and evolve through time as climate and glaciological conditions change. Such knowledge is a prerequisite to fully understand the blue ice sediment archive as a record of past glacial activity.

Law glacier and Mount Acheron moraine

Law Glacier is a ~20 km wide outlet glacier that flows through the central Transantarctic Mountains from the East Antarctic ice sheet (Fig. 1). Ice thickness toward the middle of the trough ranges from 600 to 1600 m (Blankenship and others, 2012). Surface ice flow velocity along the trunk of the glacier averages upward of 25 m a⁻¹ and decreases sharply at the margins (Rignot and others, 2011) (Fig. 1). Mount Acheron creates an embayment along the lateral margin of the glacier into which ice and sediment flows. Mount Acheron moraine is accumulating along the south side of Law Glacier ~20 km downstream of the polar plateau. The moraine is ~100 km² extending ~15 km downstream from Mount Acheron and >5 km from the active Law Glacier margin to Lewis Cliffs Ice Tongue and several other unnamed ice tongues. The majority of the moraine is dominated by a series of ridges and troughs that run subparallel to the main flow direction of Law Glacier. Instead of defining a straight lateral edge of flow, the ridges are curved mimicking the shape of the ice flowing from the main trunk of Law Glacier into the embayment (Fig. 1). Away from Law Glacier the moraine morphology is modified by impinging ice tongues.

Several studies have been conducted on the Mount Acheron blue ice moraine (Hagen, 1995; Scarrow and others, 2014; Sun and others, 2015; Bader and others, 2017; Kaplan and others, 2017; Graly and others, 2018a, 2018b). Cosmogenic exposure ages (¹⁰Be–²⁶Al–³He) across the moraine surface imply that sediment accumulation has been quasi-continuous since at least 300 ka (Hagen, 1995; Kaplan and others, 2017). Furthermore, salt development in the moraine's surface sediment suggests that sediment could have been accumulating for hundreds of thousands of years and major melt has not occurred here for ~10⁶ years (Graly and others, 2018a). An increasing till thickness from 0 cm at the moraine-ice margin inward to >1 m indicates that sediment continues to accumulate through time (Scarrow and others, 2014; Bader and others, 2017). Provenance studies of the pebble composition and sand size detrital zircons indicate that most of the sediment is derived locally with compositions similar to the lower Beacon Supergroup sedimentary rocks and Ferrar dolerite (Bader and others, 2017). Some areas of the moraine are dominated by sharp lithologic boundaries between laterally continuous visible bands of sandstone and dolerite. The lateral continuity of these distinct lithologies signifies stability of the moraine surface. In addition, facets and striations were noted on up to 30% of the cobble clasts indicating a subglacial origin for the sediment (Bader and others, 2017).

Geomorphic 'zones' introduced by Bader and others (2017) correspond to segments of the moraine with distinct geomorphic/provenance characteristics (Fig. 1b). Age constraints for each zone come from Kaplan and others (2017) and Graly and others (2018a). Zone 1 characteristics include hummocky topography with numerous melt ponds, <5 cm sediment cover and cosmogenic exposure ages generally <10 ka. Zone 2 characteristics include a relatively flat topography with a few subtle ridges (<2 m tall), slightly thicker sediment cover and cosmogenic exposure ages generally within the range of ~10–14 ka. There is a lack of large boulders and cobbles in this zone compared to all other zones. Zone 3 characteristics include distinctive ridge and

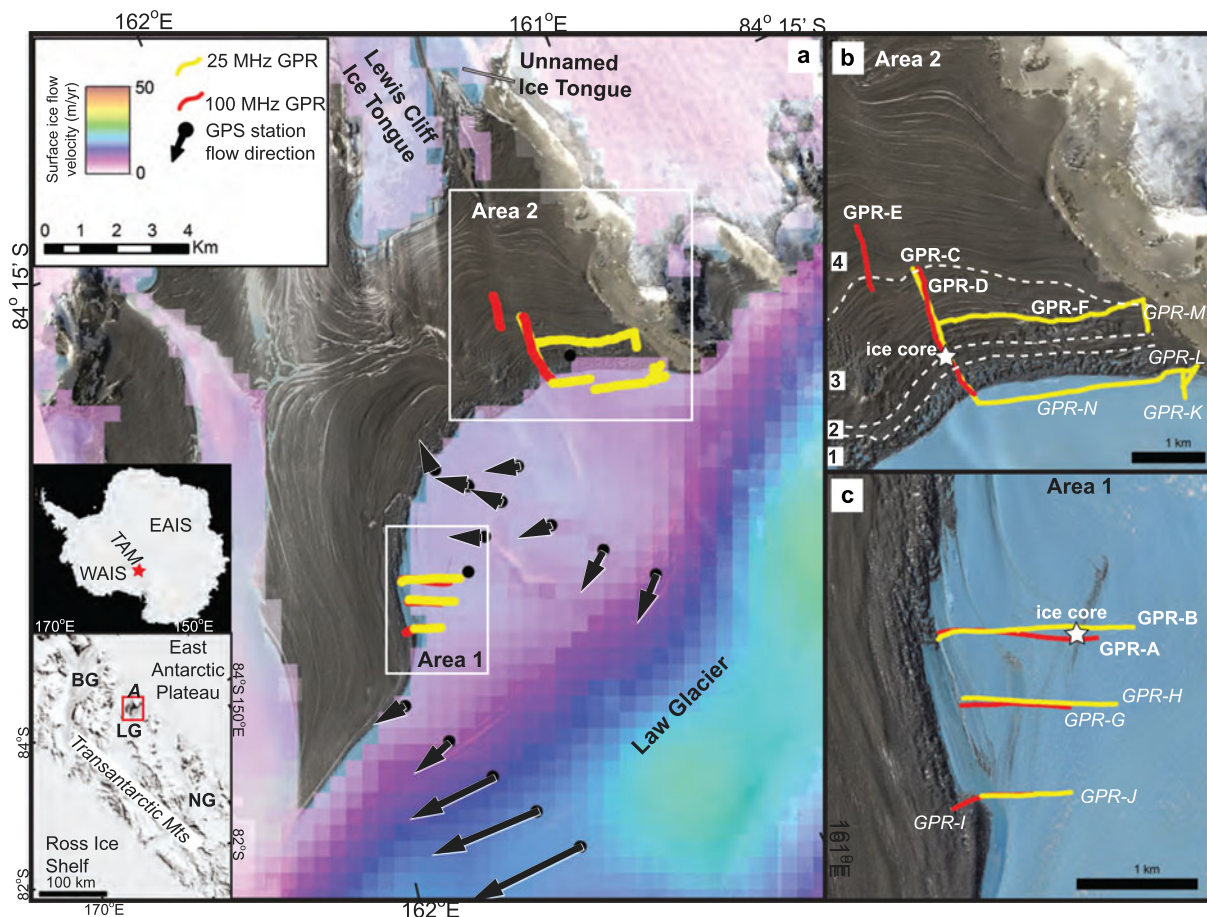


Fig. 1. (a) Satellite image of Mount Achernar moraine showing the location of the GPR transects discussed in the text. Color scale reflects surface ice flow velocity from Rignot and others (2011). Black circles mark locations of GPS stations that were deployed during the field season (2015–16), and arrows show direction and relative magnitude of ice flow velocity during the time period they were deployed. Imagery copyright 2015 DigitalGlobe, Inc. Inset maps show the location of Mount Achernar relative to Antarctica and the Transantarctic Mountains (TAM). BG, Beardmore Glacier; LG, Law Glacier; NG, Nimrod Glacier. (b) and (c) Zoomed-in image of the focus areas showing the location of the GPR lines discussed in text (bold labels) and those included in the supplementary materials (italicized text) and ice cores. Geomorphologic zones of Bader and others (2017) are numbered in (b).

trough topography, tens of cm sediment cover, and cosmogenic exposure ages typically ranging from ~14 to 55 ka. This zone has large ridges (6–10 m tall) with smaller ridges between these and superimposed on them. Two dominant tall ridges at the back of zone 3 define a boundary as all the other ridges in this zone merge into these on the upstream right lateral side of the moraine. Finally, zone 4 characteristics include a well-defined ridge and trough topography (2–6 m tall ridges), tens of cm sediment cover and cosmogenic exposure ages >55 ka. The oldest exposure ages are ~340 and ~550 ka, indicating the oldest part of the moraine is mid-to-late Quaternary in age.

Methods

Approximately 19.5 km of GPR data were collected along 14 transect lines over the moraine complex and adjoining ice during the 2015–16 field season (Fig. 1). We selected six of the lines totaling ~12 km to highlight in the text and the rest are included in the supplementary material. A MALÅ ProEx impulse radar system with either a 100 MHz unshielded antenna or 25 MHz RTA antenna for larger penetration depth was used for data acquisition. Trace positions were recorded by a single frequency code-phase GPS with absolute accuracy of 1–3 m. The system was either pulled behind a snowmobile on the ice at ~4 km h⁻¹ or carried/pulled on foot over the moraine. Individual traces were continuously recorded at a rate of four traces per second and

each trace was stacked eight times to improve the signal-to-noise ratio.

Processing of the data files was completed in ReflexW v.8.0. Prior to the application of processing filters, transect lines consisting of multiple files were edited and combined. Processing steps include dewow to remove low frequency signal or DC trends in the data, removal of duplicate traces based on GPS location, interpolation to equidistant traces, time-zero correction to adjust for variable antenna air gap when moving along the transect, background removal to remove static noise present in the whole transect, manual time-gain to improve visual appearance of deep reflectors and topographic correction. Data were not migrated due to limited knowledge of velocity structure in the subsurface and structures and point reflectors are better defined in unmigrated data. Elevation values were taken from the trace header. The average velocity value for electromagnetic wave propagation in the moraine was estimated using a hyperbolic fitting function to well-defined scatters in data and was estimated to 0.157 m ns⁻¹. This velocity lies between the known value for clean ice (0.168 m ns⁻¹) (Robin, 1975) and for till (0.1–0.12 m ns⁻¹) (Neal, 2004). Range resolution, i.e. minimum vertical distance to discriminate between two objects is estimated from $\lambda/4$ where λ is the wavelength (m) of the transmitted signal. This gives a range resolution of ~1.6 m for the 25 MHz antenna and ~0.4 m for the 100 MHz antenna. The horizontal resolution is determined by the first Fresnel zone in unmigrated data and can be estimated from $\sqrt{d\lambda/2}$ where d is the depth (Jol, 2009).

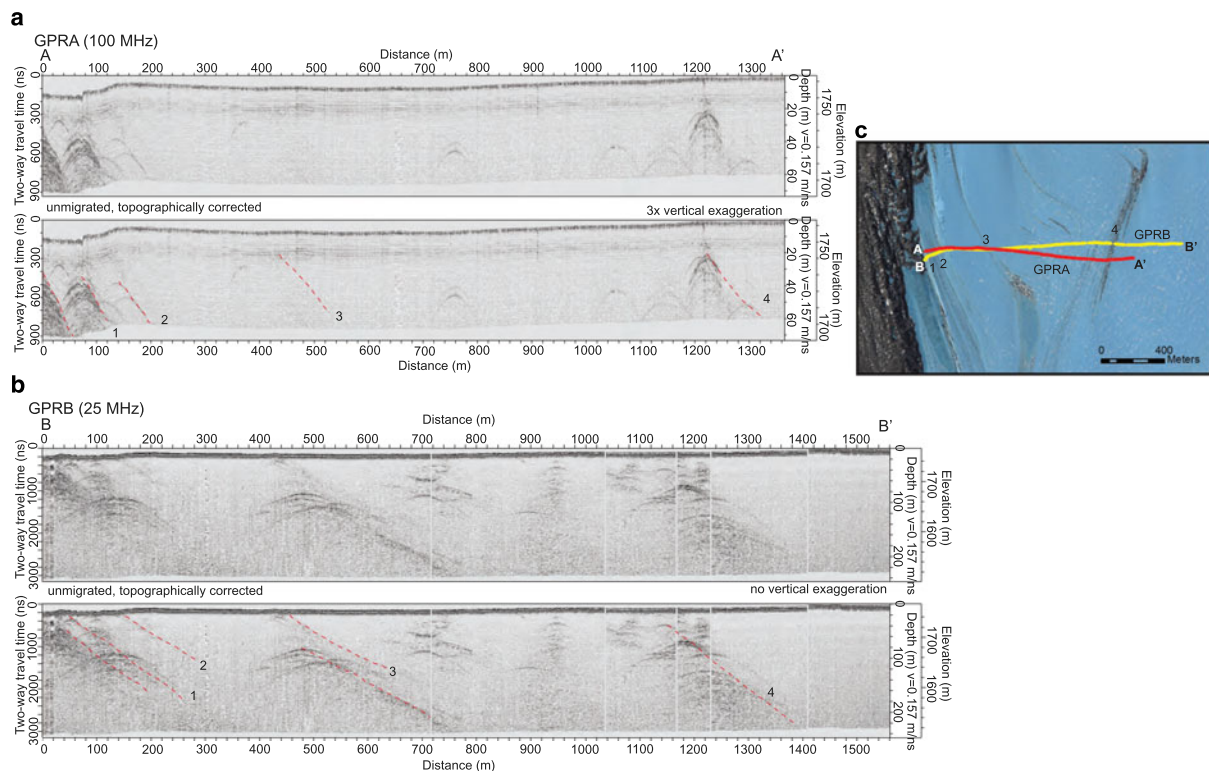


Fig. 2. GPR radargrams in area 1. (a) The 100 MHz transect and (b) the 25 MHz transect. Both profiles in each set are not migrated and are topographically corrected. The interpretation of the internal structure is shown on the lower one. The red dashed line traces the debris planes that are created from the stacked hyperbolas. The numbers in (b) correspond to distinct debris bands on the surface of the satellite image (c). Imagery copyright 2015 DigitalGlobe, Inc.

GPS stations were deployed at 15 locations in order to measure surface ice flow velocity near the Mount Acheran moraine over a 24 d period during the December 2015 field season. GPS data were collected using Trimble NetR9 receivers and Zephyr geodetic antennas. Receivers collected both hourly and daily data files at 1 and 15 s intervals, respectively. GPS data were processed using the Trimble Business Center (TBC) v2.7 software package.

Results

GPR transects were collected in two areas at Mount Acheran: area 1 where debris bands emerge on the surface of the margin of Law Glacier; and area 2, which encompasses the upstream half of the moraine (Fig. 1). Both 100 and 25 MHz transects were collected in each of these areas with the intent of producing radargrams that illustrate the deepest resolvable reflections beneath the surface and the shallower structure at a higher resolution. Transect lines were oriented both parallel and perpendicular to the ridge structure in order to get a 3-D sense of the internal structure. Two main types of reflections are identified in the radargrams, a prominent deep subhorizontal reflector and sub-parallel, steeply dipping planes, consisting of stacked hyperbolas. There are also scattered hyperbolas throughout the radargrams that do not define a plane, as well as chaotic reflection patterns. Areas that lack reflections are interpreted as clean ice or ice with debris below the resolution of the antenna (small diameter and/or low concentration).

Area 1

In area 1, six GPR transects extend from the moraine-ice boundary to the outermost visible debris band emerging on the surface of the active Law Glacier (Fig. 1). Transects GPR-A (100 MHz) and GPR-B (25 MHz) are described here (Fig. 2) and the others

are included in the supplementary material (Figs S1 and S2). The widest debris bands on the glacier surface (labeled 1–4 in Fig. 2c) correspond to the most well-defined planes in the GPR data. Many of the planes of stacked reflectors can be identified as deep as 150 m below the surface and can be traced to the surface where they are represented by thin bands of debris that have sublimated out of the ice along these ice-rich debris planes (Figs 2c and 3b).

Area 2

Ridge perpendicular transects

Six transects (25 and 100 MHz) were collected perpendicular to the ridge structure. Three are discussed in text, GPR-C, GPR-D and GPR-E (Figs 4 and 5) and the rest (GPR-K, -L and -M) are included in the supplementary material (Fig. S3). Multiple types of reflections are identified in the ridge perpendicular transects. A relatively continuous subhorizontal reflection is identified at depth in GPR-C (Fig. 4), emerging from below the depth of the radargram at ~600 m along the transect. By ~800 m along the transect the reflection is relatively flat lying for the remainder of the distance.

Above the deepest reflection, steeply dipping reflections produced by stacked hyperbolas and scattered hyperbolas are visible in both the 25 MHz (GPR-C) and 100 MHz datasets (GPR-D) (Figs 4 and 5). Variations in the presence and strength of these reflections are related to the four geomorphic zones introduced above. Steeply dipping planar reflections are poorly defined to absent in zone 1, except at ~160 m along the GPR-C transect (Fig. 4) which marks the boundary between the clean active Law Glacier and debris-rich ice of the moraine. This plane at the moraine-ice boundary extends to the surface below the first topographic ridge of the moraine. Scattered hyperbolas are present below debris cover of the moraine surface in the first

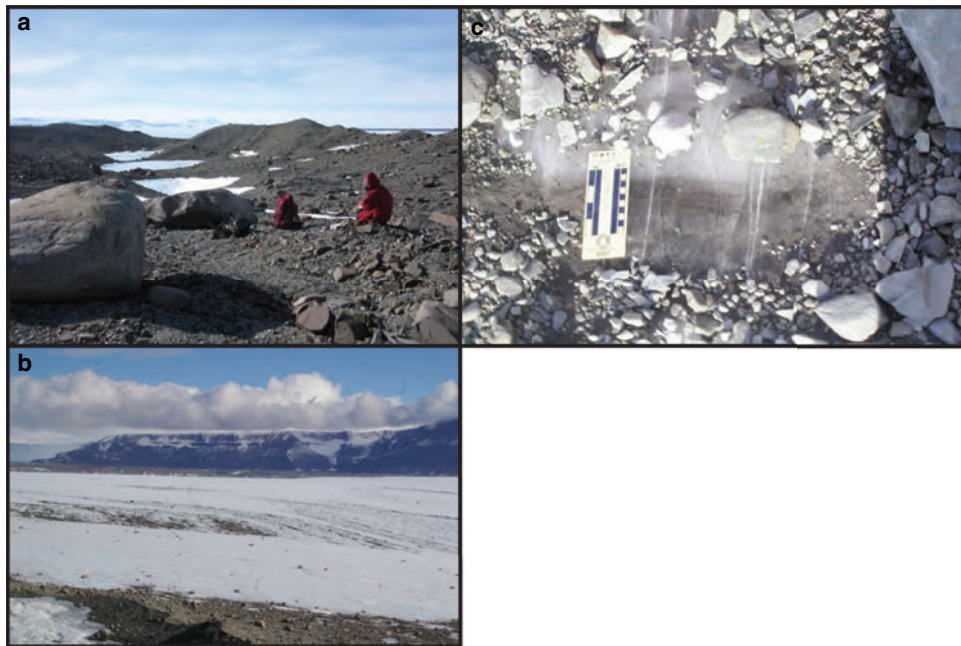


Fig. 3. (a) Image of moraine surface in zone 1 illustrating the large difference in the size of the debris at the surface. (b) View of area 1 where spaced debris bands are emerging at the surface. (c) Image of till in ice below the surficial debris in zone 1.

550 m of the transect (Figs 4 and 5). Near the zone 1/2 boundary in GPR-D (Fig. 5), the hyperbolas appear to be more clearly stacked and define faint planes that extend to the surface at a topographic ridge. Most cannot be traced beyond a depth of ~100 m. Dipping reflection planes of stacked hyperbolas continues into zone 2. Most can be traced to subdued ridges on the surface and extend to depth, at least 20–60 m below the surface, but are only visible in GPR-D (Fig. 5). Scattered hyperbolas that do not define a plane are also present, mostly at the beginning of zone 2 (Fig. 4c).

The number of dipping reflection planes increases almost two-fold in zone 3 compared to zone 2 and the average distance between the them decreases by almost half. The dip angle of these reflection planes is also slightly steeper than those in zone 2 (Fig. 5). The surface topography of zone 3 is dominated by a distinct ridge-trough topography with ridges ranging from 2 to 10 m high (Bader and others, 2017). Dipping reflections appear to cluster and emerge at the surface in association with the larger ridges. In the first 900 m of zone 3, reflections can only be traced to ~100 m depth below the surface, while those in the last 300 m asymptotically approach the deep subhorizontal reflector that is identified in GPR-C (Fig. 4).

A separate 100 MHz radargram (GPR-E) extends GPR-D transect into zone 4 (Fig. 5b). Distinct reflections are masked in this transect due to noise and likely related to increasing till thickness on the moraine surface. A few dipping planes can be identified at the zone 3/4 transition. Dip angles of the reflection planes appear to increase from zone 3 to those in the initial part of zone 4. Most of what can be identified in this zone is very faint scattered hyperbolas.

Ridge parallel transect

Two ridge parallel transects were collected in area 2 (Fig. 1). GPR-F is discussed in the text (Fig. 6) and the other is included in the supplementary material (Fig. S3). GPR-F is approximately perpendicular to the transects shown in Figures 4 and 5, intersecting GPR-C at ~1390 m (noted by star in Fig. 4). A relatively continuous subhorizontal reflection is noted at depth in GPR-F. This is the same reflection horizon noted in GPR-C. It is relatively flat lying except for where it approaches bedrock at the base of Mount

Achernar and is inclined upward. The reflection extends along the length of the profile, except from ~2000 to 2900 m where the trace cannot be differentiated from noise in the radargram. Above this, many of the subhorizontal reflections can be traced for considerable lengths but cannot be traced along the entire transect. The subhorizontal reflections intersect with the dipping reflection planes in GPR-C. For example, the subhorizontal reflection at ~30 m depth at the beginning of GPR-F is the same as the dipping reflection plane at ~1400 m in GPR-C (denoted by black triangle in Figs 4 and 5). Individual hyperbolas occur along and scattered between the reflections.

Discussion

In order to understand the architecture and formation of the Mount Achernar blue ice moraine and how it may translate to similar or identical features in other locations, we consider: (1) the physical meaning of different types of reflections, (2) if the bedrock topography is a controlling feature in blue ice moraine formation and (3) the significance of internal architecture to the temporal development of moraine-forming processes.

Reflection interpretations

Deep continuous subhorizontal reflection

We interpret the deep relatively continuous subhorizontal reflection identified in GPR-C and GPR-F to be a bedrock surface. This is based on our observation that the reflection can be traced to exposed bedrock of Mount Achernar (Fig. 6 and Fig. S3). It is likely that till overlies this interface and may cause the reflection to be difficult to trace in some places. We use the clearly identifiable bedrock surface at ~140 m depth in the beginning of GPR-F to determine where the bedrock surface is in GPR-C where they intersect at ~1390 m distance. In GPR-C (Fig. 4), the boundary between the bedrock surface and the overlying debris show continuity of reflections above it and a lack of reflections beneath it. Away from exposed bedrock at the base of Mount Achernar, the bedrock surface at depth is easiest to identify at the beginning of GPR-F (Fig. 6). Here there is a distinct difference

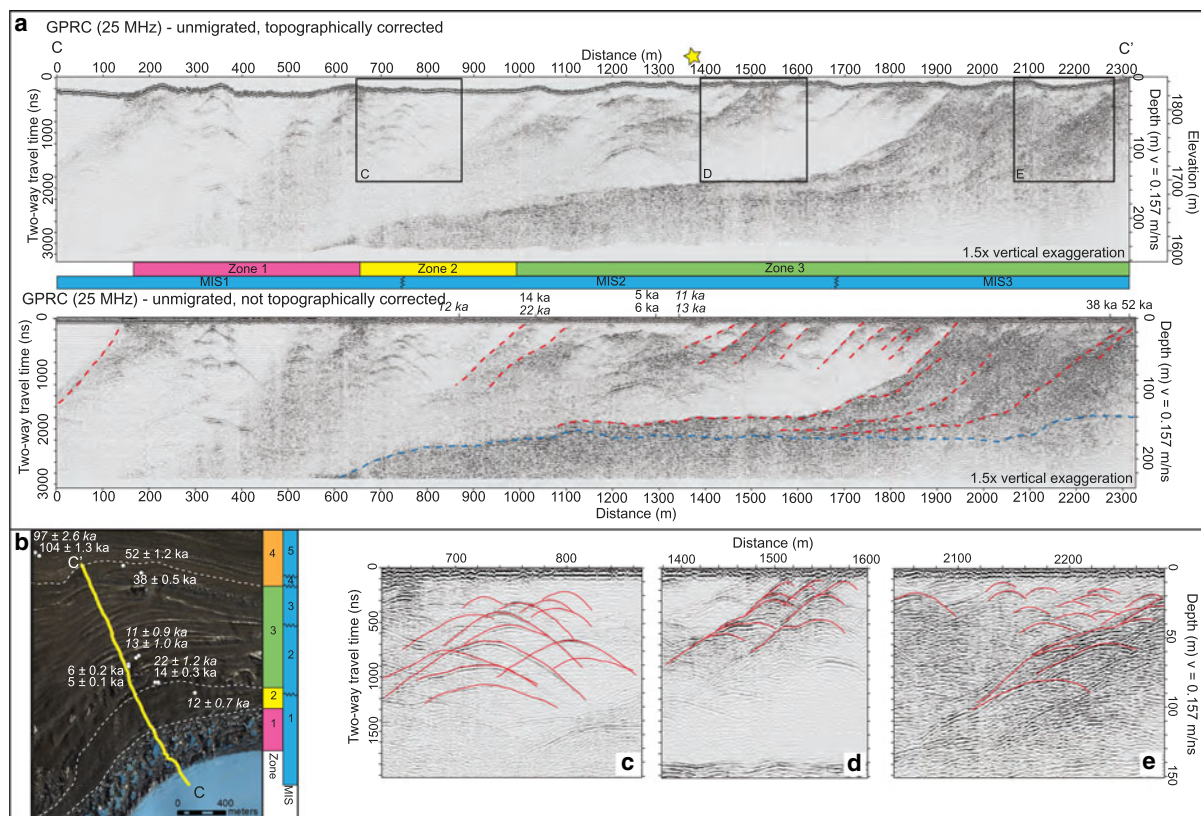


Fig. 4. GPR-C transect. (a) The upper line is the processed radargram and the lower has the interpretations on it. Red dashed lines are debris planes and the blue dashed line is the bedrock surface. Yellow star at ~ 1390 m is the intersection of GPR. MIS, marine isotope stage. (b) Satellite image indicating the location of the GPR-C transect and nearby ^{10}Be ages (regular text) and ^3He ages (italicized text) (Kaplan and others, 2017) and geomorphic zones (Bader and others, 2017). Panels C, D and E highlight different structures identified in (a): (c) scattered hyperbolae, (d) stacked hyperbolae creating a plane and (e) high-density hyperbolae and stacked hyperbolae representing a large amount of debris present in the ice in the latter part of the transect -F. Imagery copyright 2015 DigitalGlobe, Inc.

in the trace signature between clean ice and the underlying bedrock surface (Fig. 6b).

Scattered hyperbolae

Scattered hyperbolae are identified in almost all of the GPR transects that were collected. These individual hyperbolae represent point reflectors within the ice (Daniels, 2004) and we interpret them as individual cobbles/boulders contained within the ice. Faceted and striated boulders are present across the moraine surface (Fig. 3a) and are emerging in the blue ice areas of Law Glacier, therefore we assume they exist at depth within the ice producing the scattered hyperbolae identified in the radargrams.

Dipping reflections

Dipping reflections have been noted in all of the transects that run perpendicular to the moraine ridge structure (GPR-A, -B, -C and -D; Fig. 1). These dipping reflections consist of stacked hyperbolae and therefore we interpret them to represent planes of debris entrained within the ice. These planes are most prevalent in the second half of GPR-C and GPR-D (Figs 4 and 5). This pattern is consistent with parallel bands of debris-rich ice visible on the surface in area 1 (Figs 2 and 3b). Concentration of sediment in the debris bands is $\sim 1\%$ as determined by evaluation of mass of sediment per volume ice in ice cores collected in area 1 and zone 2 of area 2 (Graly and others, 2018b) (Fig. 1b, 1c). As illustrated in Figure 2, not all debris bands visible on the ice surface are imaged with the GPR, therefore it is very likely the debris load in the ice is greater than that suggested by the radargrams.

Shallow subhorizontal reflections

Shallow subhorizontal reflections are only noted in transects that are subparallel to the moraine ridge structure (Fig. 6 and Fig. S3).

In particular, they are noted within the ice above the bedrock surface in GPR-F and are interpreted to represent the 3D extension of the dipping reflections in GPR-C. These reflections are continuous and can be traced laterally for hundreds of meters.

Chaotic reflections

Zone 4 is characterized by a lack of consistent reflections in the radargram. Based on the presence of dipping debris bands noted in other zones and the significant amount of debris on the surface (upward of 1 m thick), there must be debris in the subsurface. We hypothesize that the amount of subsurface debris has become so large that all of the reflections interfere with each other resulting in clutter in the radargrams and no consistent hyperbolic reflections. A lack of clean ice in the subsurface does not allow for the discrimination of debris-rich ice therefore what we see is a lot of noise in the radargram.

Moraine formation

Are subglacial topographic shelves a prerequisite for moraine inception?

Extensive blue ice moraines like the one at Mount Acherar are not common and we speculate that embayments downstream of nunataks and shelf-like subglacial topography may be key controlling factors in moraine inception and preservation. Based on the bedrock reflection present in GPR-C, -F, -K, -L, -M and -N (Figs 4, 6 and Fig. S3), we can map a shallow bedrock surface with a low dip angle beneath the moraine in area 2 (Fig. 7b). In order to create the profile, we assume that ice thickness decreases to 0 at the back of the moraine where exposed bedrock is intersected and combine our data with radar data from IceBridge HiCARS2 L2 Geolocated Ice Thickness dataset (Blankenship

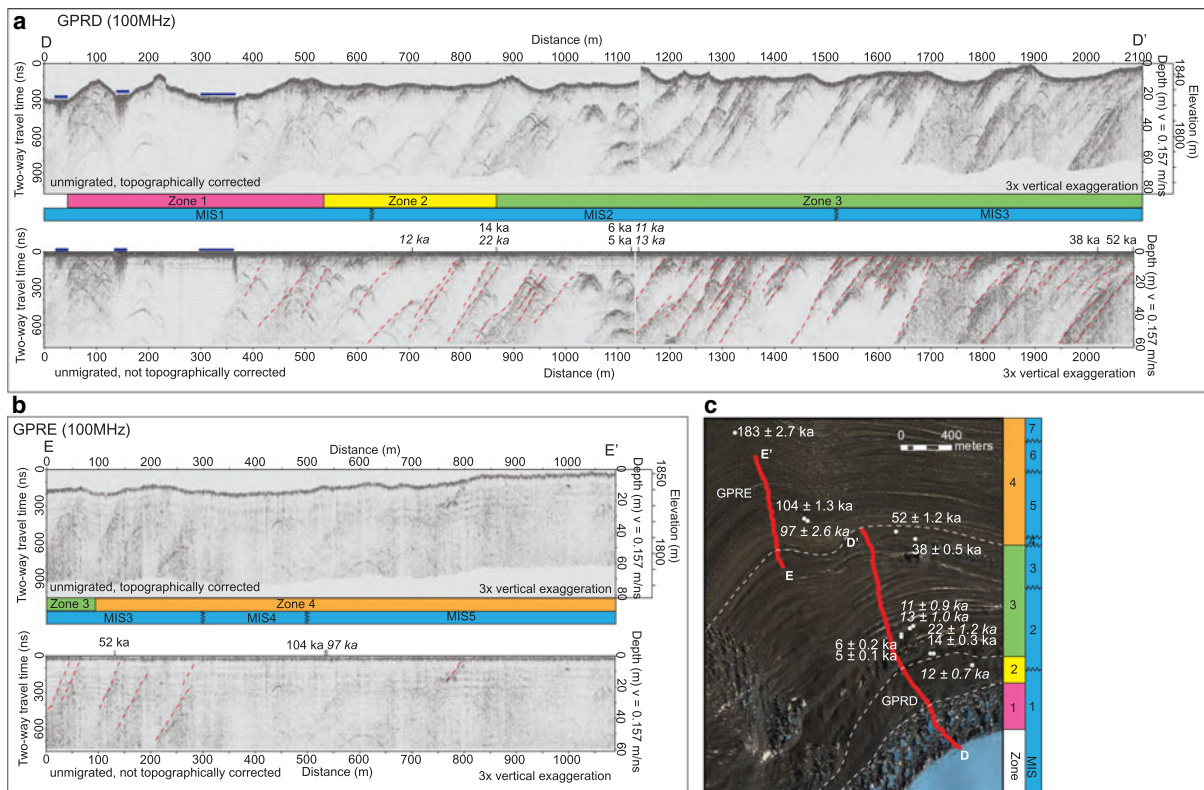


Fig. 5. 100 MHz GPR transects in area 2. (a) GPR-D radargram. (b) GPR-E radargram which is an extension of GPR-D. In both (a) and (b), the internal structure is interpreted on the lower profile. The red dashed lines highlight debris planes identified by stacked hyperbolae. (c) Satellite image indicating the location of the transects and nearby ^{10}Be ages (regular text) and ^3He ages (italicized text) (Kaplan and others, 2017) and geomorphic zones (Bader and others, 2017) MIS, marine isotope stage. Imagery copyright 2015 DigitalGlobe, Inc.

and others, 2012) collected along Law Glacier (Fig. 7). We also calculate bedrock elevation by subtracting ice thickness values from surface elevation values extracted from a digital elevation model (DEM) derived from Digital Globe, Inc. stereoscopic imagery and provided by the Polar Geospatial Center. We illustrate the presence of a bedrock shelf on which the blue ice moraine is situated by creating a simplified bedrock elevation profile (Fig. 7c). The shelf-like geometry is consistent with exposed surrounding topography where resistant sills of Ferrar dolerite often produce shelves. Further investigation of the underlying bedrock topography at other large blue ice moraines is necessary to test the speculation that a shelf-like topography is a controlling factor in moraine inception and preservation.

Lateral accretion model

Previous research on meteorite accumulation in blue ice areas has suggested that debris is brought to the surface through the upward movement of ice as it encounters a barrier and is left behind as the ice is subsequently sublimated (e.g. Cassidy and others, 1992; Harvey, 2003). Physical models of ice flow in blue ice areas by Corti and others (2008) also demonstrate the upward flow of internal ice layers in the presence of a barrier like a nunatak. These models can be interpreted to suggest that moraines develop where the entire ice column turns upward as it reached the bedrock barrier with the oldest, deepest ice exposed at the back of the moraine. Based on the internal architecture revealed by the GPR data, combined with exposure ages from the Mount Achernar moraine surface, we add substantial new evidence to support the hypothesis by Bader and others (2017) that the debris accumulates laterally after being entrained subglacially and brought up to the surface because of high ablation rates near nunataks.

Several lines of evidence lead us to a model of blue ice moraine formation by lateral accretion of ice and debris layers. First, the

width of the moraine is >5 km, much greater than the thickest ice in Law Glacier (~ 1100 m), therefore it is not possible for the moraine to represent the entire upward turning of the thickness of Law Glacier. Second, till thickness of supraglacial sediment increases from <5 cm near the active ice moraine margin to >1 m in the back of the moraine (Scarrow and others, 2014; Bader and others, 2017), supporting the idea that the moraine developed over time and not in a single event. Third, exposure ages (Kaplan and others, 2017) and boron concentration values (Graly and others, 2018a) across the moraine suggest that the debris on the surface has been accumulating quasi-continuously over at least 300 ka, with age increasing with distance from the present Law Glacier margin, and thus not in a single event. Finally, the debris planes identified in the ridge perpendicular GPR transects are similar in structure to steeply dipping shear planes or thrust sheets noted to form in ice under compression elsewhere in polar regions (e.g. Hambrey and Müller, 1978; Chinn, 1994; Huddart and Hambrey, 1996; Glasser and others, 2003; Hambrey and Glasser, 2011).

The development of debris-rich thrust sheets in ice has been noted by previous researchers mostly at the toe of glaciers where compressional stresses occur (e.g. Hambrey and Müller, 1978; Chinn, 1994; Huddart and Hambrey, 1996; Glasser and others, 2003; Hambrey and Glasser, 2011). Many of these thrust sheets are associated with debris-rich ridges on the ice surface that develop where debris emerges along planes and accumulates on the surface. We can trace the debris planes in the GPR transects in area 2 to debris covered ridges as well. In addition, the thrust sheets described in previous studies dip steeply ($>45^\circ$) up glacier and trace to the bed in a listric manner (Hambrey and Glasser, 2011). Similarly, the debris planes in this study dip up glacier reaching toward the bed, although not quite as steeply. Whether each debris plane at Mount Achernar can be considered

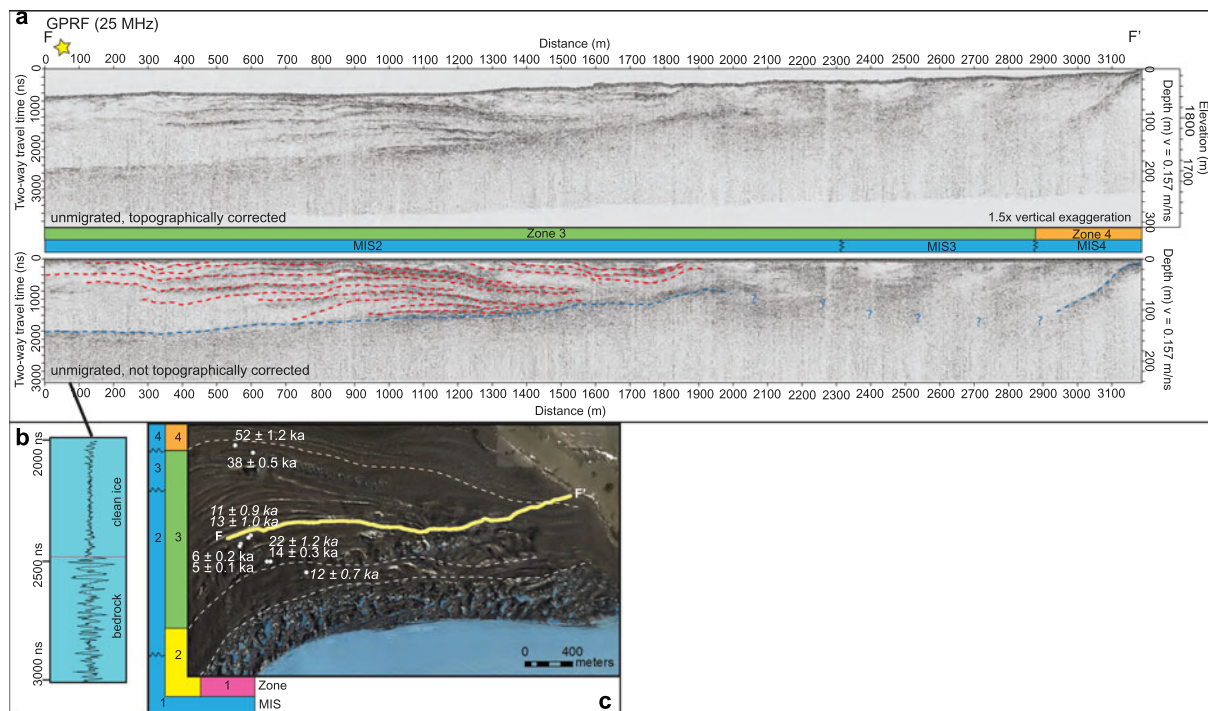


Fig. 6. (a) GPR-F radargram. (a) Interpretation of the internal stratigraphy is done on the bottom radargram. The red dashed line is the debris plane surface within the ice and the dashed blue line is the bedrock surface. Due to noise in the radargram, the bedrock surface signal is lost in the right half of the transect. This transect extends from the cliff face of Mount Achernar to GPR-C (Fig. 4) and runs mostly parallel to the ridge structure of the moraine as seen in the satellite image (c). (b) Trace signature at ~ 90 m along the transect illustrating the change in amplitude signal between ice and bedrock. (c) Satellite image indicating the location of the transects and nearby ^{10}Be ages (regular text) and ^3He ages (italicized text) (Kaplan and others, 2017) and geomorphic zones (Bader and others, 2017) MIS, marine isotope stage. Imagery copyright 2015 DigitalGlobe, Inc.

a thrust sheet, like those at the toes of the glaciers, cannot be determined with the current data.

We note the likelihood of weak compressional stresses present at Mount Achernar based on the change in surface ice flow velocity values from Law Glacier into the moraine. A combination of surface ice flow data from Rignot and others (2011) and our GPS stations indicates that the highest surface ice flow velocity in the vicinity of Mount Achernar is down the center of Law Glacier, but there is a component of ice flow extending away from the main flow into the embayment where the moraine sediment accumulates (Fig. 1a). Surface ice flow values decrease from ~ 20 to 25 m a^{-1} in the main trough to $\sim 0 \text{ m a}^{-1}$ at the margin between the active ice and moraine. We suggest that these compressional stresses are a component in the development of thrust planes. This in addition to sublimation of the ice, brings debris from depth to the surface, controlling the lateral accretion of ice and debris to form the moraine. Corti and others (2008) showed that debris will only be brought to the surface in blue ice settings when there is both compressional stresses and sublimation of the ice. Modeling work is required to more rigorously evaluate the balance of processes.

Temporal evolution

Variations in spacing and thickness of the debris bands through time may have influenced moraine development. Not all debris entrained in the ice is captured in the radargram, therefore our interpretations are based on the largest debris bands. In area 1, visible debris bands on the ice surface are spaced from 10 to >100 m apart and the width of the bands varies from ~ 2 to 30 m. Most of these debris bands are not visible in subsurface GPR data indicating low concentration of debris in the ice and/or small particle sizes. In area 2, the GPR radargram shows few distinct debris bands in the subsurface of zone 1, which was deposited over the past 6 ka. Given that the majority of bands

are too thin to be imaged in area 1, we suspect this pattern also continues beneath zone 1 (Fig. 3c). In zone 2, faint debris bands are present in the 100 MHz radargram, spaced ~ 20 – 40 m apart and extend to subdued ridges on the surface. Exposure ages indicate that till began accumulating to form this zone ~ 10 – 14 ka. Spacing between bands decreases substantially in zone 3 to ~ 5 – 20 m, with a few that are 50 m apart. Sediment here began accumulating after 55 ka.

Combining the variations in debris band concentration across the moraine with cosmogenic exposure ages (Kaplan and others, 2017), we can show the rate of development of the moraine through lateral accretion of the shear planes has not been consistent over the past ~ 180 ka. If we assume the debris bands associated with the ridges on which there are exposure ages are shear planes, using the distance between the two debris planes and the age, we can make a rough calculation to illustrate the changing accretion rate. If our assumption is correct, the lowest rates of accretion occur toward the middle of the moraine, where zone 3 transitions to zone 4 ~ 50 ka (Fig. 8). Here rates are $\sim 3.5 \text{ m ka}^{-1}$. This is where there is a large amount of debris in the subsurface as identified in the GPR radargram and also where some of the largest ridges of the moraine are located (Fig. 4a). The accretion rate increases slightly ~ 100 ka in zone 4 to $\sim 6 \text{ m ka}^{-1}$. The highest rates of lateral accretion occur in the first ~ 1500 m of the moraine, in zone 1, zone 2, and the first part of zone 3, where the rates exceed 40 m ka^{-1} . This first order approximation shows that accumulation rates in this moraine may vary by an order of magnitude over time.

Changing basal conditions

We can apply our model of lateral accretion of subglacially entrained debris to speculate about changes in basal conditions over time. In order to do this, we need to know when and

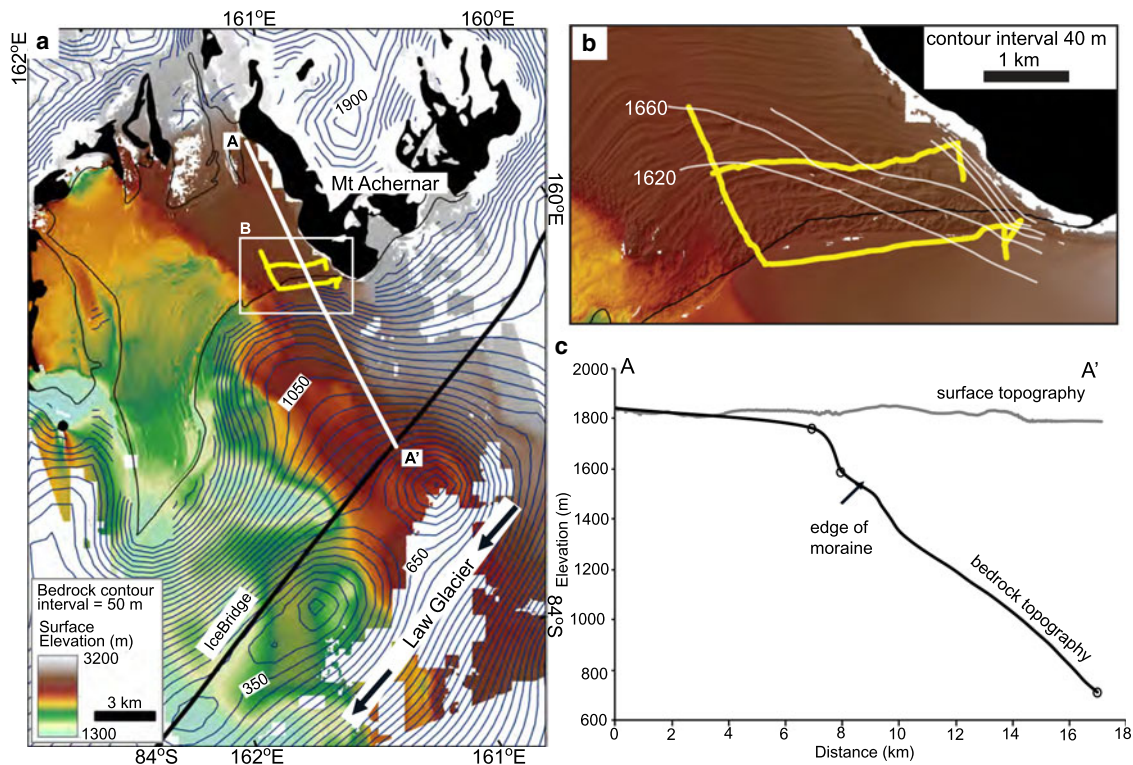


Fig. 7. (a) Surface DEM of Mount Acheron moraine and Law Glacier. Contour represents the bedrock topography based on Bedmap2 dataset excluding the area beneath the moraine. Black polygons are exposed bedrock. Black line running up Law Glacier is the location of the IceBridge dataset. (b) Bedrock contour map of bedrock below the moraine based on values from the GPR transects. (c) Cross-section line showing bedrock elevation from the back of the moraine to the middle of Law Glacier. Elevations are extracted from 25 MHz GPR transects and the IceBridge dataset. Bedrock underneath the moraine forms a shelf >1600 m elevation that sits above the trough of Law Glacier. Imagery copyright 2015 DigitalGlobe, Inc.

where the sediment was entrained. Both of these values are not well constrained for Mount Acheron, but we can make some educated assumptions to support our speculations.

In order to calculate when debris was initially at the bedrock–ice interface, we need to know sublimation rates and ice thicknesses throughout the moraine. A first order sublimation rate (d) is calculated using the following equation:

$$d = \frac{\rho_t \times x}{\rho_i \times t}$$

where ρ_t is the density of till on the moraine surface (g cm^{-3}), x is the thickness of debris (cm), ρ_i is the density of till in ice (g cm^{-3}) and t is the age (years).

Debris thickness ranges from <5 cm near the ice–moraine margin to >1 m in zone 4 (Sarrow and others, 2014; Bader and others, 2017). Published till density values range from 1.6 to 2.0 g cm^{-3} depending on the amount of weathering (Schueler, 2000). Average soil bulk density in Taylor Valley is 1.8 g cm^{-3} (Toner and others, 2003). We have estimates of the density of till in ice from shallow ice cores that were collected from thin debris bands in the emerging zone and zone 2 (Graly and others, 2018b). Calculated average values from these ice cores range from ~ 0.001 to 0.006 g cm^{-3} (Table S1). We use an average value for ρ_i (0.0035 g cm^{-3}).

Calculated sublimation rates range from 0.20 to 0.52 cm a^{-1} with the highest rates closest to the ice–moraine margin (Table 1; Fig. 8). These values are an order of magnitude larger the range of values from debris-covered ice in Beacon Valley where Ng and others (2005) calculated sublimation values of 0.001 – 0.01 cm a^{-1} and an order of magnitude lower than measured rates from Taylor Glacier (Bliss and others, 2011). Because sublimation rates will decrease as debris cover thickens (Schäfer and others, 2000), values for Mount Acheron moraine

zones 2–4 are likely maximum values, which would bring them closer to those from Beacon Valley.

To calculate the time it takes for debris to move from the bedrock–ice interface to the surface, we use the calculated sublimation rate and ice thickness/bedrock depth values from the GPR transects (Table 1). Due to the differing sublimation rates and depths to bedrock throughout the moraine, an estimate on the age at which debris at the surface was last at the bedrock–ice interface varies spatially. Exposure ages are added to the travel time to get an approximate time at which the debris was at the bed. The calculated ages most likely represent maximum potential ages because sublimation rates most likely changed over time (Table 1; Fig. 8). Maximum potential ages for debris to be near the bedrock interface based on the estimated sublimation rates range from 35 ka in zone 1 to 151 ka in zone 4 (Fig. 8).

These values do not represent the time of entrainment, as they only represent the time since debris was at the bedrock–ice interface. In order to link the internal stratigraphy of the moraine to changes in basal conditions we need to make an assumption about the location of debris entrainment and ice flow velocity. Graly and others (2018b) estimated that the basal entrainment zone for debris at Mount Acheron is at most, ~ 30 – 50 km upstream. Basal ice flow velocity values are most likely a fraction of surficial ice flow velocity values which range from 25 m a^{-1} in the middle of Law Glacier to 0 m a^{-1} near the ice–moraine contact. Based on model output from Golledge and others (2013), basal ice flow velocities for Law Glacier are $<1 \text{ m a}^{-1}$. Using a minimum and maximum distance for basal entrainment (30–50 km) and assuming a basal ice flow velocity of 0.5 m a^{-1} , it would take ~ 60 – 100 ka for sediment to be transported to the moraine. Adding this to the age when debris was at the bedrock–ice interface results in ages that reflect a timing of entrainment from 95 to 251 ka (Table 1).

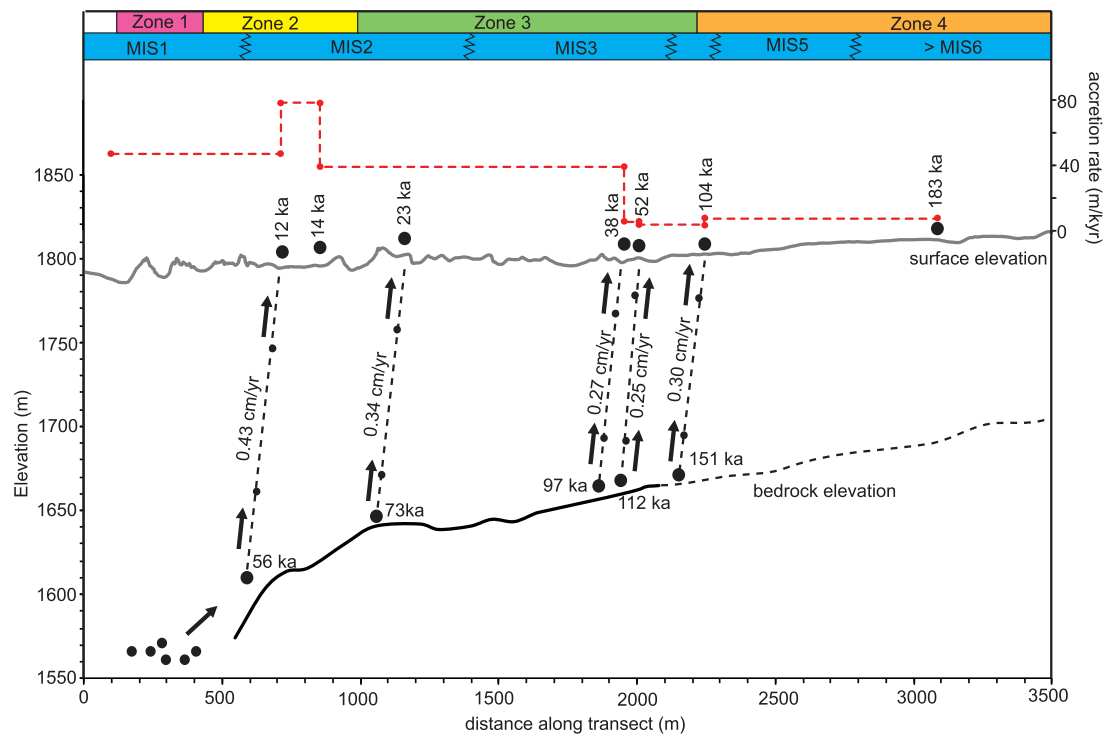


Fig. 8. Graph illustrating the changing accretion rates (dashed red line) across the moraine based on distance between sediment exposure ages (black dots on surface). Topographic profile of the moraine surface is extracted from the DEM. Bedrock elevation is from GPR-C. Rates between the surface and bedrock elevation are calculated sublimation rates (see text for explanation) and ages at the bedrock surface are maximum times when debris at the surface was at the base of the ice based upon the sublimation rate, ice thickness, and surface exposure ages.

Table 1. Sublimation rates and travel time from bedrock–ice interface to surface

	t (years)	x (cm)	ρ_t (g cm^{-3})	ρ_i (g cm^{-3})	d (cm a^{-1})	Depth to bedrock (m)	Approximate travel time (years)	Approximate time since at bed (ka)	Approximate time since entrainment (ka)
Zone 1	3000 ^a	4	1.8	0.0035	0.69	>220	32 000	35	95–135
Zone 2	12 000	10	1.8	0.0035	0.43	190	44 000	56	114–154
Zone 3	23 000	15	1.8	0.0035	0.34	170	50 000	73	130–170
	38 000	20	1.8	0.0035	0.27	160	59 000	97	157–197
Zone 4	52 000	25	1.8	0.0035	0.25	150	60 000	112	168–208
	104 000	60	1.8	0.0035	0.30	140	47 000	151	211–251

^aApproximate age estimated from data in Graly and others (2018a, 2018b) and Kaplan and others (2017).

If the entrainment ages are reasonable first order approximations, we can use them to link the timing of changes in basal conditions of Law Glacier to the internal architecture of the moraine. Isotopic data from ice samples suggest that sediment within the active Law Glacier was entrained under cold-based conditions and sediment within the moraine was entrained under warm-based conditions (Graly and others, 2018b). In zones 1 and 2 of the moraine where there is limited debris, entrainment likely occurred during the MIS5 interglacial. Whereas zone 3 and the younger part of zone 4 are dominated by debris planes and based on our entrainment age estimates sediment was entrained during a period with much colder surface conditions (MIS6). This analysis suggests that higher debris concentration, particularly in the form of debris bands in the internal architecture of the moraine was entrained during glacial maxima. Overall, a working hypothesis derived from these data is that there is an inverse relationship between surface and basal temperatures. The continuity of the moraine geomorphology indicates that ice thickness changes must have been minimal (tens of meters) across this timeframe.

An alternative hypothesis to explain the change in debris concentration throughout the subsurface structure of the moraine is that it is related to proximity of the bedrock surface. The overall

decrease in debris concentration with time may reflect the change in debris derived from the underlying bedrock shelf, that we postulate is a Ferrar dolerite sill and sediment entrained under thicker ice farther upstream. The decreasing internal debris concentration toward Law Glacier is coincident with a change in till provenance. Ferrar pebbles are found in greater abundance in zone 4 where debris is most concentrated in sub-moraine ice; for comparison, sedimentary rocks of the lower formations of the Beacon Supergroup become more abundant in zones 2 and 3 where debris concentration declines. It seems likely that the longer travel distance may also cause debris to become more dispersed throughout the ice.

Conclusions

We present some of the first published GPR data on the subsurface structure and evolution of an extensive blue ice moraine at the edge of the polar plateau in the Transantarctic Mountains. Multiple types of reflections can be identified in GPR transects across the area where debris has recently emerged on the surface of the active marginal Law Glacier and the Mount Achernar sediment moraine sequence. Steeply dipping reflections, consisting of stacked hyperbolae are the most prominent throughout both

areas. Beneath these reflections and scattered point reflectors, a prominent subhorizontal reflection exists that we interpret as a bedrock surface that dips slightly toward the main trough of Law Glacier.

We interpret the dipping reflectors to be debris bands that originate at depth and carry sediment to the surface where it is then sublimated out of the ice. The pattern of dipping reflections integrated with surface exposure ages in Kaplan and others (2017) and boron concentration data in Graly and others (2018a) suggests that ice and debris are accreting laterally to form this moraine. The rate of lateral accretion does not appear to be constant through time and shows an order of magnitude range in variability (2 to >40 m ka⁻¹). The surface topography appears to reflect these changes in accretion rates. The lowest rates occur where there is a well-developed ridge-trough topography (back of zones 3 and 4) and the highest where the topography is either flat or hummocky (zones 1, 2 and first part of zone 3). In addition, changes in the subsurface structure reflect variable basal conditions through time. By assuming basal ice velocity values, we can roughly estimate when debris in different parts of the moraine were entrained. Based on the estimates, we speculate that higher concentrations of debris and more debris bands were subglacially entrained during times of relatively cold climate (MIS 6). Alternatively, the changing concentration and composition may reflect the location from which the debris originated, below the moraine or farther up ice.

In order for blue ice moraines to develop a long, relatively continuous record, we postulate that there must be: (1) basal conditions upstream that produce debris entrainment, (2) an area of high ablation releasing the entrained debris, (3) lateral accretion as a result of sublimation, compressional ice flow, and a bedrock shelf in an embayment that together result in topographic steering and (4) minimal change in ice thickness over glacial/interglacial cycles. Substantial changes in ice thickness and surface elevation would disturb the moraine architecture, and perhaps even cause reversed flow and drainage of the moraine system out of the embayment (Bader and others, 2017; Kaplan and others, 2017). Not all blue ice areas covered by debris appear to have all these conditions, but those that do are an important archive of ice-sheet history.

Supplementary material. The supplementary material for this article can be found at <https://doi.org/10.1017/jog.2019.83>.

Acknowledgements. This research was supported by the National Science Foundation Office of Polar Programs grant PLR-1443433 and PLR-1443213. S.J. Townsend and G. Johnston provided helpful suggestions and discussion in the development of this paper. We thank the United States Antarctic Program, Crary Lab staff, Kenn Borek Air Ltd., and mountaineer Peter Braddock for fieldwork support and the Polar Geospatial Center for satellite imagery. The final version of this paper benefited greatly from anonymous reviewers. This is LDEO contribution 8361.

References

- Ackert Jr RP and 5 others (2011) West Antarctic Ice Sheet elevations in the Ohio Range: geologic constraints and ice sheet modeling prior to the last highstand. *Earth and Planetary Science Letters* **307**(1–2), 83–93. doi: [10.1016/j.epsl.2011.04.015](https://doi.org/10.1016/j.epsl.2011.04.015).
- Ackert Jr RP and 6 others (2013) Controls on interior West Antarctic Ice Sheet Elevations: inferences from geologic constraints and ice sheet modeling. *Quaternary Science Reviews* **65**, 26–38. doi: [10.1016/j.quascirev.2012.12.017](https://doi.org/10.1016/j.quascirev.2012.12.017).
- Altaier M, Herpers U, Delisle G, Merchel S and Ott U (2010) Glaciation history of Queen Maud Land (Antarctica) reconstructed from in-situ produced cosmogenic ¹⁰Be, ²⁶Al and ²¹Ne. *Polar Science* **4**, 42–61. doi: [10.1016/j.polar.2010.01.001](https://doi.org/10.1016/j.polar.2010.01.001).
- Bader NA, Licht KJ, Kaplan MR, Kassab C and Winckler G (2017) East Antarctic ice sheet stability recorded in a high-elevation ice-cored moraine. *Quaternary Science Reviews* **159**, 88–102. doi: [10.1016/j.quascirev.2016.12.005](https://doi.org/10.1016/j.quascirev.2016.12.005).
- Bintanja R (1999) On the glaciological, meteorological, and climatological significance of Antarctic blue ice areas. *Reviews of Geophysics* **37**(3), 337–359. doi: [10.1029/1999RG900007](https://doi.org/10.1029/1999RG900007).
- Blankenship DD and 12 others (2012, updated 2017) IceBridge HiCARS 2 L2 Geolocated Ice Thickness, Version 1. [IRMCR2_20131119_04]. Boulder, Colorado USA. NASA National Snow and Ice Data Center Distributed Active Archive Center. doi: [10.5067/9EBR2T0VXUDG](https://doi.org/10.5067/9EBR2T0VXUDG) (Accessed 1 November 2017).
- Bliss AK, Cuffey KM and Kavanaugh JL (2011) Sublimation and surface energy budget of Taylor Glacier, Antarctica. *Journal of Glaciology* **57** (204), 684–696. doi: [10.3189/002214311797409767](https://doi.org/10.3189/002214311797409767).
- Bromley GRM, Hall BL, Stone JO, Conway H and Todd CE (2010) Late Cenozoic deposits at Reddy Glacier, Transantarctic Mountains: implications for former thickness of the West Antarctic Ice Sheet. *Quaternary Science Reviews* **29**, 384–398. doi: [10.1016/j.quascirev.2009.07.001](https://doi.org/10.1016/j.quascirev.2009.07.001).
- Campbell S and 6 others (2013) Radar-detected englacial stratigraphy in the Pensacola Mountains, Antarctica: implications for recent changes in ice flow and accumulation. *Annals of Glaciology* **54**(63), 91–100. doi: [10.3189/2013AoG63A371](https://doi.org/10.3189/2013AoG63A371).
- Cassidy W, Harvey R, Schutt J, Delisle G and Yanai K (1992) The meteorite collection sites of Antarctica. *Meteoritics* **27**, 490–525.
- Chinn TJ (1994) Polar glacier margin and debris features. *Memorie della Società Geologica Italiana* **46**, 25–44.
- Corti G, Zeoli A, Belmaggio P and Folco L (2008) Physical modeling of the influence of bedrock topography and ablation on ice flow and meteorite concentration in Antarctica. *Journal of Geophysical Research* **113**(F1). doi: [10.1029/2006JF000708](https://doi.org/10.1029/2006JF000708).
- Daniels DJ (2004) *Ground Penetrating Radar*, 2nd Edn., London: The Institute of Engineering and Technology.
- Denton GH, Bockheim JG, Wilson SC, Leide JE and Andersen BG (1989) Late quaternary ice-surface fluctuations of Beardmore Glacier, Transantarctic Mountains. *Quaternary Research* **31**, 183–209. doi: [10.1016/0033-5894\(89\)90005-7](https://doi.org/10.1016/0033-5894(89)90005-7).
- Fogwill CJ, Hein AS, Bentley M and Sugden DE (2011) Do blue-ice moraines in the Heritage Range show the West Antarctic ice sheet survived the last interglacial? *Palaeogeography, Palaeoclimatology, Palaeoecology* **335–336**, 61–70. doi: [10.1016/j.palaeo.2011.01.027](https://doi.org/10.1016/j.palaeo.2011.01.027).
- Fukui K, Sone T, Strelin JA, Torielli CA and Mori J (2008) Dynamics and GPR stratigraphy of a polar rock glacier on James Ross Island, Antarctic Peninsula. *Journal of Glaciology* **54**(186), 445–451. doi: [10.3189/002214308785836940](https://doi.org/10.3189/002214308785836940).
- Glasser NF, Hambrey MJ, Etienne JL, Jansson P and Pettersson R (2003) The origin and significance of debris-charged ridges at the surface of Storglaciären, Northern Sweden. *Geografiska Annaler. Series A, Physical Geography* **85**(2), 127–147. doi: [10.1111/1468-0459.00194](https://doi.org/10.1111/1468-0459.00194).
- Golledge NR and 12 others (2013) Glaciology and geological signature of the Last Glacial Maximum Antarctic ice sheet. *Quaternary Science Reviews* **78**, 225–247. doi: [10.1016/j.quascirev.2013.08.011](https://doi.org/10.1016/j.quascirev.2013.08.011).
- Graly JA, Licht KJ, Druschel GK and Kaplan MR (2018a) Polar desert chronologies through quantitative measurements of salt accumulation. *Geology* **46**(4), 351–354. doi: [10.1130/G39650.1](https://doi.org/10.1130/G39650.1).
- Graly JA, Licht KJ, Kassab CM, Bird BW and Kaplan MR (2018b) Warm-based basal sediment entrainment and far-field Pleistocene origin evidenced in central Transantarctic blue ice through stable isotopes and internal structures. *Journal of Glaciology* **64**(244), 185–196. doi: [10.1017/jog.2018.4](https://doi.org/10.1017/jog.2018.4).
- Hagen EH (1995) *A Geochemical and Petrological Investigation of Meteorite Ablation Products in Till and Ice of Antarctica* (Dissertation). The Ohio State University, 525 p.
- Hambrey MJ and Glasser NF (2011) Sediment entrainment, transport, and deposition. In Singh VP, Singh P and Haritashya UM ed. *Encyclopedia of Snow, Ice and Glaciers*. Springer Nature, The Netherlands, 984–1003.
- Hambrey MJ and Müller F (1978) Structures and ice deformation in the White Glacier, Axel Heiberg Island, Northwest Territories, Canada. *Journal of Glaciology* **20**(82), 41–66. doi: [10.3189/S0022143000021213](https://doi.org/10.3189/S0022143000021213).
- Harvey R (2003) The origin and significance of Antarctic Meteorites. *Chemie der Erde Geochemistry* **63**, 93–147. doi: [10.1078/0009-2819-00031](https://doi.org/10.1078/0009-2819-00031).
- Hein AS and 9 others (2016) Evidence for the stability of the West Antarctic ice sheet divide for 1.4 million years. *Nature Communications* **7**. doi: [10.1038/ncomms10325](https://doi.org/10.1038/ncomms10325).

- Higgins JA and 8 others** (2015) Atmospheric composition 1 million years ago from blue ice in the Allan Hills, Antarctica. *PNAS* **112**(22), 6887–6891. doi: [10.1073/pnas.1420232112](https://doi.org/10.1073/pnas.1420232112).
- Huddart D and Hambrey MJ** (1996) Sedimentary and tectonic development of a high-arctic, thrust-moraine complex: Comflossbreen, Svalbard. *Boreas* **25**, 227–243. doi: [10.1111/j.1502-3885.1996.tb00639.x](https://doi.org/10.1111/j.1502-3885.1996.tb00639.x).
- Hui G and 12 others** (2014) Mapping blue-ice areas in Antarctica using ETM + and MODIS data. *Annals of Glaciology* **55**(66), 129–137. doi: [10.3189/2014AoG66A069](https://doi.org/10.3189/2014AoG66A069).
- Jamieson SSR, Sugden DE and Hulton NRJ** (2010) The evolution of the subglacial landscape of Antarctica. *Earth and Planetary Science Letters* **293**, 1–27. doi: [10.1016/j.epsl.2010.02.012](https://doi.org/10.1016/j.epsl.2010.02.012).
- Jol H** (2009) *Ground Penetrating Radar Theory and Applications*. Elsevier Science, New York.
- Joy K, Fink D, Storey B and Atkins C** (2014) A 2 million year glacial chronology of the Hatherton Glacier, Antarctica and implications for the size of the East Antarctic Ice Sheet at the Last Glacial Maximum. *Quaternary Science Reviews* **83**, 46–57. doi: [10.1016/j.quascirev.2013.10.028](https://doi.org/10.1016/j.quascirev.2013.10.028).
- Kaplan MR and 9 others** (2017) Middle to Late Pleistocene stability of the central East Antarctic Ice Sheet at the head of Law Glacier. *Geology* **45** (11), 963–966. doi: [10.1130/G39189.1](https://doi.org/10.1130/G39189.1).
- Korotikh EV and 7 others** (2011) The last interglacial as represented in the glaciochemical record from Mount Moulton Blue Ice Area, West Antarctica. *Quaternary Science Reviews* **30**(15–16), 1940–1947. doi: [10.1016/j.quascirev.2011.04.020](https://doi.org/10.1016/j.quascirev.2011.04.020).
- Krissek L and 9 others and ANDRILL-MIS Science Team** (2007) Sedimentology and Stratigraphy of the AND-1B Core, ANDRILL McMurdo Ice Shelf Project, Antarctica. *Terra Antarctica* **14**(3), 185–222.
- Mackay SL, Marchant DR, Lamp JL and Head JW** (2014) Cold-based debris-covered glaciers: evaluating their potential as climate archives through studies of ground-penetrating radar and surface morphology. *Journal of Geophysical Research Earth Surface* **119**, 2505–2540. doi: [10.1002/2014JF003178](https://doi.org/10.1002/2014JF003178).
- McKay R and 10 others** (2009) The stratigraphic signature of the late Cenozoic Antarctic Ice Sheets in the Ross Embayment. *GSA Bulletin* **121** (11–12), 1537–1561. doi: [10.1130/B26540.1](https://doi.org/10.1130/B26540.1).
- Moore JS and 7 others** (2006) Interpreting ancient ice in a shallow ice core from the South Yamato (Antarctica) blue ice area using flow modeling and compositional matching to deep ice cores. *Journal of Geophysical Research* **111**(D16). doi: [10.1029/2005JD006343](https://doi.org/10.1029/2005JD006343).
- Neal A** (2004) Ground-penetrating radar and its use in sedimentology: principles, problems and progress. *Earth-Science Reviews* **66**, 261–330. doi: [10.1016/j.earscirev.2004.01.004](https://doi.org/10.1016/j.earscirev.2004.01.004).
- Ng F, Hallet B, Sletten RS and Stone JO** (2005) Fast-growing till over ancient ice in Beacon Valley, Antarctica. *Geology* **33**(2), 121–124. doi: [10.1130/G21064.1](https://doi.org/10.1130/G21064.1).
- Palmer EF, Licht KJ, Swope RJ and Hemming SR** (2012) Nunatak moraines as a repository of what lies beneath the East Antarctic ice sheet. In Rasbury ET Hemming SR and Riggs NR ed. *Mineralogical and Geochemical Approaches to Provenance*. Geological Society of America Special Paper, Boulder, CO, 97–104 (doi: [10.1130/2012.2487\(05\)487](https://doi.org/10.1130/2012.2487(05)487))
- Pattyn R** (2010) Antarctic subglacial conditions inferred from a hybrid ice sheet/ice stream model. *Earth and Planetary Science Letters* **295**(3–4), 451–461. doi: [10.1016/j.epsl.2010.04.025](https://doi.org/10.1016/j.epsl.2010.04.025).
- Rignot E, Mouginot J and Scheuchl B** (2011) Ice flow of the Antarctic Ice Sheet. *Science* **333**, 1427–1430. doi: [10.1126/science.1208336](https://doi.org/10.1126/science.1208336).
- Robin G** (1975) Radio-echo sounding: glaciological interpretations and applications. *Journal of Glaciology* **15**(73), 49–64. doi: [10.3189/S0022143000034262](https://doi.org/10.3189/S0022143000034262).
- Scarrow JW, Balks MR and Almond PC** (2014) Three soil chronosequences in recessional glacial deposits near the polar plateau, in the Central Transantarctic Mountains, Antarctica. *Antarctic Science* **26**(5), 573–583. doi: [10.1017/S0954102014000078](https://doi.org/10.1017/S0954102014000078).
- Schäfer JM and 6 others** (2000) The oldest ice on Earth in Beacon Valley, Antarctica: new evidence from surface exposure dating. *Earth and Planetary Science Letters* **179**(1), 91–99. doi: [10.1016/S0012-821X\(00\)00095-9](https://doi.org/10.1016/S0012-821X(00)00095-9).
- Schueler T** (2000) *The Compaction of Urban Soil: The Practice of Watershed Protection*. Ellicott City, MD: Center for Watershed Protection, pp. 210–214.
- Shean DE and Marchant DR** (2010) Seismic and GPR surveys of Mullins Glacier, McMurdo Dry Valleys, Antarctica: ice thickness, internal structure and implications for surface ridge formation. *Journal of Glaciology* **56**(195), 48–64. doi: [10.3189/002214310791190901](https://doi.org/10.3189/002214310791190901).
- Sinisalo A and 5 others** (2007) Inferences from stable water isotopes on the Holocene evolution of Scharffenbergbotnen blue-ice area, East Antarctica. *Journal of Glaciology* **53**(182), 427–434. doi: [10.3189/002214307783258495](https://doi.org/10.3189/002214307783258495).
- Sinisalo A and Moore JC** (2010) Antarctic blue ice areas (BIAs) – towards extracting paleoclimate information. *Antarctic Science* **22**(2), 99–115. doi: [10.1017/S0954102009990691](https://doi.org/10.1017/S0954102009990691).
- Spaulding NE and 9 others** (2013) Climate archives from 90 to 250 ka in horizontal and vertical ice cores from the Allan hills Blue Ice Area, Antarctica. *Quaternary Research* **80**(3), 562–574. doi: [10.1016/j.yqres.2013.07.004](https://doi.org/10.1016/j.yqres.2013.07.004).
- Staiger JW and 6 others** (2006) Plio-Pleistocene history of Ferrar Glacier, Antarctica: implications for climate and ice sheet stability. *Earth and Planetary Science Letters* **243**(3–4), 489–503. doi: [10.1016/j.epsl.2006.01.037](https://doi.org/10.1016/j.epsl.2006.01.037).
- Sun T and 7 others** (2015) Lost cold Antarctic deserts inferred from unusual sulfate formation and isotope signatures. *Nature Communications* **6**, 7579. doi: [10.1038/ncomms8579](https://doi.org/10.1038/ncomms8579).
- Todd C, Stone J, Conway H, Hall B and Bromley G** (2010) Late Quaternary evolution of Reedy Glacier, Antarctica. *Quaternary Science Reviews* **29**, 1328–1341. doi: [10.1016/j.quascirev.2010.02.001](https://doi.org/10.1016/j.quascirev.2010.02.001).
- Toner JD, Sletten RS and Prentice ML** (2003) Soluble salt accumulations in Taylor Valley, Antarctica: implications for paleolakes and Ross Sea Ice Sheet dynamics. *Journal of Geophysical Research: Earth Surface* **118**, 198–215. doi: [10.1029/2012JF002467](https://doi.org/10.1029/2012JF002467).
- Whillans IM and Cassidy WA** (1983) Catch a falling star: meteorites and old ice. *Science* **222**(4619), 55–57. doi: [10.1126/science.222.4619.55](https://doi.org/10.1126/science.222.4619.55).
- Whitehouse PL, Bentley MJ and Le Brocq AM** (2012) A deglacial model for Antarctica: geological constraints and glaciological modelling as a basis for a new model of Antarctic glacial isostatic adjustment. *Quaternary Science Reviews* **32**, 1–24. doi: [10.1016/j.quascirev.2011.11.016](https://doi.org/10.1016/j.quascirev.2011.11.016).
- Winter K and 10 others** (2016) Assessing the continuity of the blue ice climate record at Patriot Hills, Horseshoe Valley, West Antarctica. *Geophysical Research Letters* **43**(5), 2019–2026. doi: [10.1002/2015GL066476](https://doi.org/10.1002/2015GL066476).
- Winther J, Jespersen MN and Liston GE** (2001) Blue-ice areas in Antarctica derived from NOAA AVHRR satellite data. *Journal of Glaciology* **47**(157), 325–334. doi: [10.3189/172756501781832386](https://doi.org/10.3189/172756501781832386).
- Zekollari H, Goderis S, Debaille V, van Ginneken M and Gattacceca J and ASTER Team** (2019) Unravelling the high-altitude Nansen blue ice field meteorite trap (East Antarctica) and implications for regional palaeo-conditions. *Geochimica et Cosmochimica Acta* **248**, 289–310. doi: [10.1016/j.gca.2018.12.035](https://doi.org/10.1016/j.gca.2018.12.035).